DOI 10.1007/s10593-020-02730-4

Chemistry of Heterocyclic Compounds **2020**, *56*(6), 776–785

8-Ethynylxanthines as promising antiproliferative agents, angiogenesis inhibitors, and calcium channel activity modulators

Pavel Arsenyan[1]*, Jelena Vasiljeva[1], Ilona Domracheva[1], Iveta Kanepe-Lapsa[1]

[1] *Latvian Institute of Organic Synthesis,*
21 Aizkraukles St., Riga LV-1006, Latvia; e-mail: pavel@osi.lv

Published in Khimiya Geterotsiklicheskikh Soedinenii, 2020, *56*(6), 776–785

Submitted October 16, 2019
Accepted after revision April 15, 2020

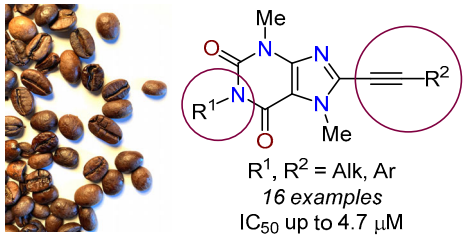

Synthetic procedures for the preparation of 8-ethynylxanthines by treating 8-bromocaffeine and 8-bromopentoxifylline with terminal acetylenes were elaborated. Certain ethynylxanthine derivatives exhibit high *in vitro* antiproliferative activity against a panel of cancer cell lines, matrix metalloproteinase and *in vitro* angiogenesis inhibitory activity. Ca^{2+} channel blocking and agonist activity of the synthesized ethynylxanthines was discussed based on data obtained on the H9C2, SH-SY5Y, and A7R5 cell lines.

Keywords: caffeine, xanthine, angiogenesis, calcium channel, cancer, cytotoxicity.

Cancer is one of the main causes of death in economically developed countries.[1] In 2017, 1.68 million new cancer cases and 600,920 cancer deaths were projected to occur only in the US, which has a population of approximately 324 million people.[2,3] In clinical practice, treatment of cancer involves a wide range of chemotherapy drugs. However, most of them exhibit various side effects, high toxicity, and moderate selectivity. Therefore, the development of a new generation of selective anticancer agents with low toxicity is one of the main goals for medicinal chemistry and pharmaceutical industry. Despite advanced studies on the elaboration of anticancer drugs, treatment outcome for malignant brain tumors remains poor. Unfortunately, most of the promising antitumor drugs used against brain tumors in clinical trials had limited impact on human survival, which was due to the lack of efficient drug delivery to the target in the central nervous system (CNS) at a sufficient concentration.[4–6]

The increased interest in xanthines stems from the prevalence of this heterocyclic system in many natural substances and from the ability of methylxanthine derivatives to penetrate the blood-brain barrier (BBB). Xanthines are an important class of compounds with a wide range of pharmacological effects, including anticancer, antiHIV, anticoagulant, antispasmodic, and antibacterial activity. Currently, several anticancer drugs based on the structure of natural purine analogs are used in clinical practice (e.g., cladribine, fludarabine, mercaptopurine, thioguanine, clofarabine, and nelarabine). These compounds are the first-line therapeutic agents for malignant hematologic diseases. Agents with 80% cure rate after a course of monochemotherapy are considered to have a therapeutic effect of complete remission. Purine analogs, which include intracellular enzyme inhibitors, act as antimetabolites by replacing the natural nucleosides in DNA and RNA synthesis. Unfortunately, these drugs show a wide range of side effects, and their high treatment costs limit their potential use in clinical practice.

To minimize side effects, antitumor drugs based on the caffeine core are currently being developed. Caffeine derivatives possess CNS expression as Ca^{2+} agonists or antagonists. Recent studies have shown that daily consumption of caffeinated coffee can lower mouth and brain cancer formation up to 39%. Additionally, it reduces the risk of cervical cancer development in women. Caffeine reduces the possibility of prostate cancer formation in men by 60% and can prevent breast, colon, and hepatic cancer.[7–9] Caffeine also enhances doxorubicin and cisplatin activity in metastatic carcinomas, lymphomas, and bone and soft tissue sarcomas.[10,11] Additionally, caffeine effectively inhibits breast cancer resistance protein (BCRP)-mediated multidrug resistance (MDR) in the MCF-7 and MCF-7/MX100 (mitoxantrone-resistant) cell lines.[12] One of the advantages of caffeine derivatives is their ability to cross the BBB and

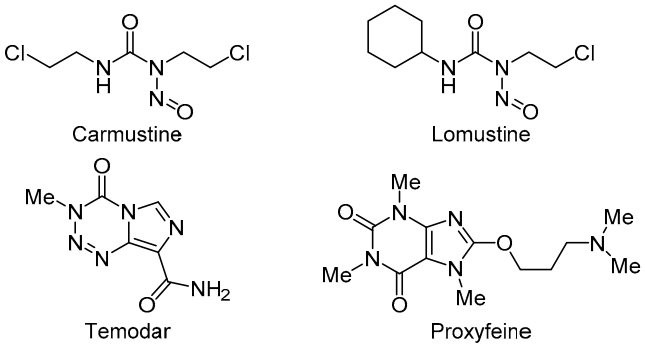

Figure 1. Structures of some drugs used in neuro-oncology.

enter CNS. Consequently, these compounds have potential to treat malignant diseases in the brain, such as neuroblastoma and glioblastoma multiforme.[13] By contrast, some drugs used in neuro-oncology (e.g., Temodar, carmustine (BCNU), lomustine (CCNU), Fig. 1) have a limited ability to cross the BBB and are highly toxic.

Caffeine is absorbed rapidly and completely from the intestinal tract, making it 100% bioavailable. Antitumor agents have been developed from various caffeine analogs, including 8-[3-(dimethylamino)propoxy]caffeine (Proxyfeine). However, introduction of these compounds into the clinic in the EU and the US has been hindered due to their high levels of toxicity (LD_{50} 355 mg/kg) and numerous serious side effects. In Russia and other countries, Proxyfeine is used in chemotherapy for cancer patients with a high risk of brain metastases and in the rehabilitation of the metastatic lesions to the brain, as well as during the early stages of cancer metastasis treatment.

Based on these considerations, we have contemplated the design of 8-ethynylxanthines. Here, to address the question of whether these compounds are promising candidates for intensive studies as antitumor agents, we report the elaboration of synthetic procedures for ethynylxanthines and data on the *in vitro* antiproliferative activity in various malignant cell lines and on the matrix metalloproteinase (MMP) and angiogenesis inhibitory activity *in vitro* of these and reference compounds (caffeine, pentoxifylline, Proxyfeine, and Temodar). Because caffeine derivatives are known to act as Ca^{2+} channel modulators, we present experimental data on this activity induced by the studied compounds.

The substitution of position 8 in xanthines is a common way to prevent their oxidation during metabolism. A similar strategy was used to design the structure of Proxyfeine. This molecule consists of a caffeine core and a flexible dimethylaminopropoxy substituent at position 8. By introducing a triple bond into the linker between the caffeine moiety and an amine, we attempted to reduce molecular flexibility while increasing stability to metabolism.

Previously, ethynylxanthines were obtained by reacting 5-chlorouracil with aminoacetonitrile.[14] We decided to utilize the Pd-catalyzed cross-coupling reaction of terminal acetylenes and 8-bromocaffeine and 8-bromopentoxifylline, as it is the most common procedure for achieving this goal. Thus, caffeine and pentoxifylline were chosen as starting materials. Both xanthines were brominated using excess *N*-bromosuccinimide (NBS) in CH_2Cl_2 in analogy to a published procedure.[15] After 5 days of stirring, the desired 8-bromocaffeine (**1**) and 8-bromopentoxifylline (**2**) were isolated in almost quantitative yields (99 and 95%, respectively).

Our synthetic strategy for the introduction of the ethynyl moiety at position 8 of the xanthine core was based on Sonogashira-type coupling reactions (Table 1). We found

Table 1. General procedure toward the synthesis of compounds **3**–**18**

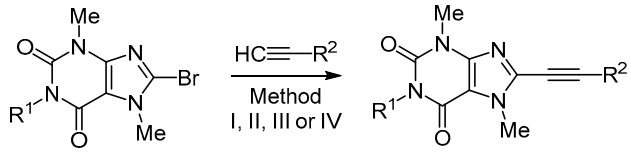

1 R = Me
2 R = $(CH_2)_4COMe$

Method I: $PdCl_2$, Ph_3P, CuI, NMP or DMF, DIEA, 50°C, 24 h
Method II: $Pd(OAc)_2$, Ph_3P, CuI, NMP or $AcNMe_2$, DIEA, 55°C, 24 h
Method III: $Pd(OAc)_2$, Ph_3P, CuI, NMP–PhMe, 1:1, DIEA, 50°C, 24 h
Method IV: $Pd(PPh_3)_4$, $PdCl_2$, Ph_3P, CuI, EtOAc, DIEA, 40°C, 2–4 h

Compound	R^1	R^2	Yield, %			
			Method			
			I	II	III	IV
3	Me	$C(Me)_2OH$	42	31	72	55
4	Me	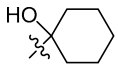		11	49	54
5	Me	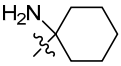	7	16	43	48
6	Me	CH_2NMe_2		4	47	58
7	Me	$CH_2N(CH_2CH_2OMe)_2$		10	30	33
8	Me	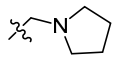	8		52	57
9	Me	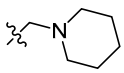			35	30
10	Me	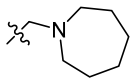			34	
11	Me	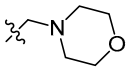			38	
12	$(CH_2)_4COMe$	$C(Me)_2OH$			44	47
13	$(CH_2)_4COMe$	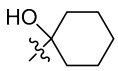			42	
14	$(CH_2)_4COMe$	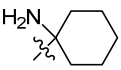			45	
15	$(CH_2)_4COMe$	$CH_2N(CH_2CH_2OMe)_2$			35	
16	$(CH_2)_4COMe$	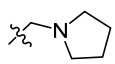			41	
17	$(CH_2)_4COMe$	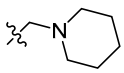			39	
18	Me	Ph			36	

that the product yields in the Pd-catalyzed cross coupling of terminal acetylenes and 8-bromoxanthines strongly depend on the nature of the catalyst and solvent. Based on the experimental data, the reaction of terminal acetylenes with compounds **1** and **2** under routine experimental conditions (methods I and II) in general led to the formation of the corresponding 8-ethynylxanthines **3**–**18** in very low yields. Surprisingly, we found that a mixture *N*-methylpyrrolidine–PhMe, 1:1 (method III) as the reaction media afforded the desired products in higher yields. Considering the goal in synthetic chemistry of developing more eco-friendly procedures, an alternative method was elaborated (method IV). Performing the procedure in nontoxic EtOAc and using 2 mol % $Pd(PPh_3)_4$ and 2 mol % $PdCl_2$ decreases the cost of the reaction and simplifies the isolation of the product.[16]

In vitro antiproliferative activity

After the preparation of a set of 8-ethynylxanthines according to our designed synthetic approach, their activity against malignant tumor cell lines was established. The *in vitro* cytotoxicity of the 8-ethynylxanthines was tested on the following monolayer tumor cell lines: MDA-MB-435s human melanoma, H9C2 rat embryo cardiomyoblasts, MCF-7 estrogen-positive human breast adenocarcinoma, HepG2 human hepatocellular carcinoma, SH-SY5Y human neuroblastoma, C6 rat glioma, U937 human histiocytic leukemia, and A549 human lung carcinoma. The results of these experiments are summarized in Table 2. Caffeine, Proxyfeine, and pentoxifylline were used as reference compounds. Although antitumor activity of Temodar is more pronounced in *in vivo* models, this drug was used as a reference compound as well. Caffeine and pentoxifylline exhibited no cytotoxic effect in all the studied cell lines. Moreover, despite the widespread use of Temodar as a drug for brain cancer treatment, the *in vitro* results showed that the compound had only modest activity against the studied tumor cell lines (IC_{50} 298 μM on SH-SY5Y neuroblastoma cells and IC_{50} 31 μM on U937 lymphoma cells). In fact, the studied malignant cells were more sensitive to Proxyfeine (IC_{50} 96–283 μM). We observed that 8-ethynylcaffeines had a strong ability to suppress cancer cell growth. Thus, caffeine derivatives **8**–**10** showed a pronounced *in vitro* antiproliferative effect on the majority of cancer cells. Moreover, these compounds were active against neuroblastoma and brain tumors (IC_{50} 8.2–14 μM on the SH-SY5Y and C6 cell lines). Notably, caffeine derivative **5** selectively inhibits lymphoma U937 cell growth (IC_{50} 5.1 μM), and derivative **8** inhibits the growth of estrogen-positive human breast adenocarcinoma MCF-7 cells (IC_{50} 5.7 μM). Piperidylmethyl derivative of pentoxifylline **17** showed high cytotoxicity against the studied cancer cells, especially on the lymphoma U937 (IC_{50} 4.7 μM) and glioma C6 (IC_{50} 7.1 μM) cell lines.

Table 2. *In vitro* cytotoxicity (IC_{50}*, μM) caused by

Compound	MDA-MB-435s	H9C2	MCF-7	HepG2	SH-SY5Y	C6	U937	A549
Caffeine	–***	–	–	–	–	–	–	–
Proxyfeine	283	–	135	–	111	96	97	–
Pentoxifylline	–	–	–	–	–	–	–	–
Temodar	515	–	–	–	298	–	31	–
3	119	141	–	–	83	261	79	239
4	–	–	–	–	–	187	95	–
5	13	41	36	96	41	15	5.1	52
6	28	57	25	28	25	28	9.2	42
7	–	–	–	–	–	–	–	–
8	8.6	75	5.7	17	8.6	11.5	26	8.6
9	14	68	14	60	14	8.5	5.7	17
10	8.2	8.2	8.2	13.7	8.2	8.2	5.5	8.2
11	–	–	–	–	–	–	124	–
12	–	22	169	86	105	277	83	188
13	–	–	259	–	116	183	85	259
14	80	46	73	96	64	20	87	78
16	7.3	9.8	4.9	12	4.9	17	12	7.3
17	19	52	11.8	26	9.5	7.1	4.7	11.8
18	122	51	44	34	17	17	13.6	85

* IC_{50} – concentration (μM) providing 50% cell killing effect (MTT).
** Tumor cell lines: MDA-MB-435s human melanoma, H9C2 rat embryo cardiomyoblasts, MCF-7 estrogen-positive human breast adenocarcinoma, HepG2 human hepatocellular carcinoma, SH-SY5Y human neuroblastoma, C6 rat glioma, U937 human histiocytic leukemia, and A549 human lung carcinoma.
*** "–" – No effect.

MMP and angiogenesis inhibition

MMPs, also known as matrixins, hydrolyze components of the extracellular matrix. These proteinases play a central role in many biological processes, such as embryogenesis, normal tissue remodeling, wound healing, and angiogenesis, and in various diseases, such as atheroma, arthritis, cancer, and tissue ulceration. MMP-2 (gelatinase A) is very active in degrading the extracellular matrix. The inhibition of MMPs by the synthesized 8-ethynylxanthines was detected using an MMP Inhibitor Fluorimetric Profiling Kit with NNGH (*N*-isobutyl-*N*-(4-methoxyphenylsulfonyl)glycyl hydroxamic acid) as a standard. According to our data, reference compounds such as caffeine, Proxyfeine, pentoxifylline, and Temodar did not inhibit any of the studied human MMPs (Table 3). By contrast, novel caffeine derivatives **3**, **11**, and **14** exhibit the ability to selectively inhibit MMP-2 (gelatinase A) up to 52%. Besides, (aminocyclohexyl)ethynyl derivative **5** inhibits MMP-10 activity up to 53%. Based on the MMP inhibition data, five compounds **3**, **5**, **11**, **14**, and **18** were chosen for *in vitro* angiogenesis inhibition studies. The *in vitro* experiments were performed on the Matrigel (BD Biosciences) human umbilical vein endothelial cell (HUVEC) tube formation model. According to the obtained experimental results, ethynylxanthines **3**, **5**, and **11** activate angiogenesis by 40–74%, whereas (aminocyclohexyl)ethynyl-substituted pentoxifylline derivative **14** and phenylethynyl-substituted caffeine derivative **18** exhibit the ability to suppress angiogenesis by 38 and 100%, respectively, at a concentration of 20 μM (Fig. 2). There is no direct correlation between angiogenesis and MMP inhibition. Accordingly, we presume that the tested compounds modulate the formation of new blood vessels by another mechanism.

Table 3. Matrix metalloproteinases and *in vitro* angiogenesis inhibition (%) caused by 8-ethynylxanthines **3**, **5**, **11**, **14**, **18**

Compound	MMP-1	MMP-2	MMP-3	MMP-7	MMP-8	MMP-9	MMP-10	MMP-12	MMP-13	MMP-14	*In vitro* inhibition,** %
NNGH* (1.3 μM)	100	100	100	7.2	100	100	100	100	100	100	
Caffeine	8.0	0	7.2	2.3	3.2	0	0	3.2	0	9.3	
Proxyfeine	1.3	0	2.0	2.5	0	0.5	0	4.6	0	7.3	
Pentoxifylline	0	0	0	1.1	0	0	0	3.5	0.6	8.4	
Temodar	6.5	0	3.8	8.5	6.5	23.1	3.1	0	5.8	13.4	
3	0	47.4	1.1	0	9.8	3.8	6.6	2.4	0	20.9	–40 ± 11
5	0	23.7	0	0	31.0	12.0	53.3	0	0	48.1	–74 ± 17
11	5.9	51.8	1.1	5.6	10.4	18.9	12.7	24.0	0	14.6	–62 ± 18
14	0	39.8	0	4.2	3.9	8.3	0	0	2.0	31.5	38 ± 8
18	0	0	20.2	1.7	4.7	2.3	1.8	3.5	0	0	100 ± 10

* *N*-Isobutyl-*N*-(4-methoxyphenylsulfonyl)glycyl hydroxamic acid.
** *In vitro* inhibition of HUVEC tube formation.

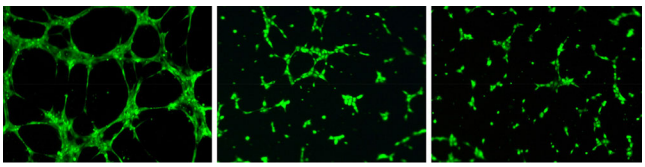

Figure 2. Inhibition of HUVEC capillary tube formation. Left – control, center – treated with compound **14**, right – treated with compound **18**.

Ca^{2+} channel agonist–antagonist modulation

Many signaling processes involved in cancer cell proliferation and movability depend on Ca^{2+} signaling. An important consequence of intracellular signaling is the increase in intracellular Ca^{2+} concentration ($[Ca^{2+}]_i$), which is well known to be a critical signal for gene expression, motility, differentiation, and survival. Cancer cell migration depends mainly on actin polymerization and the intracellular organization of various cytoskeletal proteins, which are influenced by a variety of actin-binding proteins. Actin-binding protein activity is regulated by second messengers such as phosphoinositides and Ca^{2+}.[17–19] A change in the concentration of intracellular free Ca^{2+} ($[Ca^{2+}]_i$) triggers a diverse range of cellular processes, such as muscle contraction, fertilization, secretion, and neurotransmitter release.[20] As a well-known activator of ryanodine receptor (RyR), caffeine stimulates the release of Ca^{2+} from both the skeletal and cardiac muscle sarco/endoplasmic reticulum (SR/ER).[21]

Ca^{2+} channel blocking activity

The Ca^{2+} channel blocking activity induced by the 8-ethynylxanthines was evaluated in rat cardiomyoblast (H9C2), human neuroblastoma (SH-SY5Y), and smooth muscle (A7R5) cell lines. Caffeine was used as an agonist in a cardiomyocyte model for RyR induction of Ca^{2+} release. Next, KCl was used for the intracellular Ca^{2+} mobilization through the voltage-gated L-type Ca^{2+} channel in A7R5 smooth muscle cells. Carbachol was used in neuroblastoma SH-SY5Y cells to obtain a carbachol-/IP3-sensitive Ca^{2+} store.[22]

According to our results (Table 4), the reference compounds Proxyfeine, pentoxifylline, and Temodar had a weak effect on Ca^{2+} channel activity in cardiomyoblast cells. Caffeine and Temodar exhibit an absence of antagonist properties in neuroblastoma and smooth muscle cells. By contrast, Proxyfeine is an antagonist in SH-SY5Y and A7R5 cells (IC_{50} 0.67 and 0.52 mM, respectively). Among the caffeine analogs, only caffeine derivative **5** does not block Ca^{2+} channel activity in the three studied cell lines. Compound **3** is a selective antagonist in neuroblastoma cells, whereas compounds **7** and **11** are selective antagonists in smooth muscle cells. Apparently, these derivatives predominantly induce depolarization of

Table 4. Ca^{2+} channel antagonist effect caused by 8-ethynylxanthines **3**–**18** (IC_{50}, mM)*

Compound	H9C2	SH-SY5Y	A7R5
Caffeine	Not tested	–**	–
Proxyfeine	>2	0.67 ± 0.02	0.52 ± 0.03
Pentoxifylline	1.5 ± 0.1	>2	>2
Temodar	1.5 ± 0.1	–	–
3	–	0.35 ± 0.02	>2
4	0.74 ± 0.03	0.057 ± 0.003	0.25 ± 0.02
5	–	–	–
6	0.56 ± 0.03	1.0 ± 0.2	>2
7	–	–	0.40 ± 0.03
8	0.43 ± 0.01	0.52 ± 0.01	0.41 ± 0.02
9	0.58 ± 0.03	0.60 ± 0.01	0.52 ± 0.02
10	0.36 ± 0.01	0.18 ± 0.01	0.38 ± 0.03
11	–	–	1.0 ± 0.2
12	0.89 ± 0.05	1.0 ± 0.02	0.6 ± 0.01
13	–	0.57 ± 0.02	0.52 ± 0.03
14	–	0.19 ± 0.02	0.13 ± 0.02
16	0.30 ± 0.01	0.87 ± 0.02	0.47 ± 0.01
17	0.075 ± 0.005	0.35 ± 0.02	0.28 ± 0.01
18	0.67 ± 0.03	1.0 ± 0.2	0.29 ± 0.02

* Data are presented as a mean ± SD.
** "–" – No effect.

the vascular smooth muscle cell membrane, followed by the opening of the L-type Ca^{2+} channels; however, they do not affect receptor-operated Ca^{2+} channel activity in SH-SY5Y (stimulated with carbachol) or H9C2 (stimulated with caffeine) cells. Notably, compound **4** exhibits increased selective antagonism in neuroblastoma cells (IC_{50} 0.057 mM). Pentoxifylline analogs **12**, **16**, and **17** are Ca^{2+} channel antagonists in cardiomyocytes; furthermore, the IC_{50} value of compound **17** reaches 0.075 mM in cardiomyocytes. Compound **14** showed an increase in antagonist activity in neuroblastoma and smooth muscle cells compared to pentoxifylline and do not block the Ca^{2+} channels in cardiomyocytes. Importantly, compounds with higher antiproliferative activity *in vitro* than Proxyfeine displayed Ca^{2+} channel antagonist properties. The Ca^{2+} channel antagonist activity of known antagonist of Ca^{2+} channels amlodipine (2-[(2-aminoethoxy)methyl]-4-(2-chlorophenyl)-6-methyl-1,4-dihydropyridine-3,5-dicarboxylic acid 3-ethyl 5-methyl ester) in the smooth muscle A7R5 cell line (IC_{50} 0.14 μM)[23] indicated that the studied caffeine and pentoxifylline derivatives **3**–**18** did not exhibit a strong ability to influence blood pressure.

Ca^{2+} channel agonist activity

Compounds that are not Ca^{2+} channel antagonists show agonist properties. According to our experimental data, six compounds induce the release of Ca^{2+} in the cytoplasm in a cardiomyocyte model (Figs. 3 and 4). Aminomethylethynyl-caffeine derivatives **5**, **7**, and **11** are more potent Ca^{2+} channel agonists than caffeine. These compounds stimulate a biphasic Ca^{2+} response in an early burst (to approximately 2.4 μM $[Ca^{2+}]_i$) of Ca^{2+} release from intracellular stores, which is followed by a sustained phase of Ca^{2+} influx through the cell membrane. The initial peak is not expressed in the case of caffeine. The effect of 8-[(1-aminocyclohexyl)ethynyl]caffeine (**5**) is indicated by its long and slow increase in intracellular calcium. Compounds **5**, **7**, and **11** showed agonist properties in neuroblastoma cells, with compound **5** also exhibiting a prolonged slow increase in intracellular Ca^{2+}. Notably, only compound **5** is an agonist in aortic cells (A7R5).

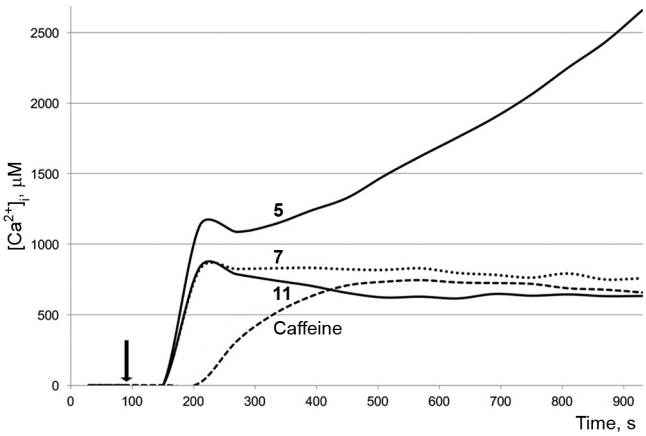

Figure 3. 8-Ethynylxanthine-induced Ca^{2+} influx in H9C2 cells. Representative traces of changes in $[Ca^{2+}]_i$ concentration in response to application of compounds **5**, **7**, **11** and caffeine (500 μM). The arrow indicates drug injection time. Each point represents the mean of four values.

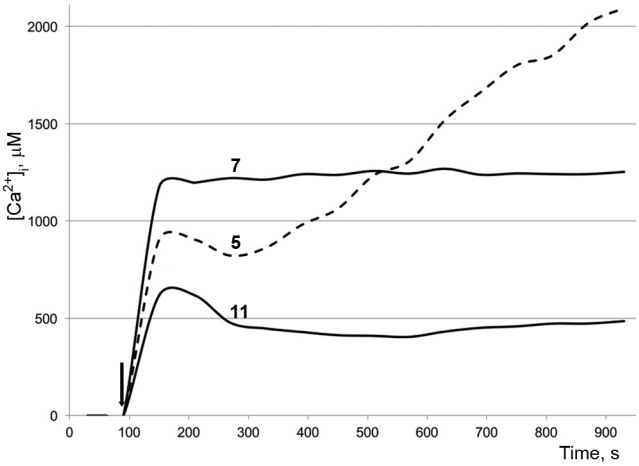

Figure 4. 8-Ethynylxanthine-induced Ca^{2+} influx in SH-SY5Y cells. Representative traces of changes in $[Ca^{2+}]_i$ concentration in response to application of compounds **5**, **7**, **11** (500 μM). The arrow indicates drug injection time. Each point represents the mean of four values.

Signaling pathway involved in intracellular Ca^{2+} release

Electrically excitable cells can utilize three major Ca^{2+} signaling pathways, namely, Ca^{2+} entry through voltage-dependent Ca^{2+} channels; release of intracellularly stored Ca^{2+} from Ca^{2+} stores bearing inositol 1,4,5-trisphosphate receptors (InsP3Rs), which are sensitive to the second messenger inositol 1,4,5-trisphosphate (InsP3); and release of Ca^{2+} from Ca^{2+} stores bearing ryanodine receptors (RyRs), which are sensitive to caffeine. These pathways have some of the best characterized tool compounds.[24,25]

We studied the possible involvement of the Gi/o/Gq/11 G protein-phospholipase C-InsP3 receptor pathway in the $[Ca^{2+}]_i$ increase in cells induced by the tested compounds. Pretreatment of cells with 2-aminoethoxydiphenyl borate (2-APB, an InsP3R inhibitor) at a dose of 100 μM for 15 min did not block the agonist effect of any compounds in any of the cell lines. This result indicates that the release of intracellularly stored Ca^{2+} by the tested compounds is not associated with the InsP3 receptors.

We further tested the role of RyRs in the compound-induced Ca^{2+} response in cells (Table 5). RyRs are responsible

Table 5. Role of ryanodine receptor (RyR)-induced Ca^{2+} response

Compound*	Ruthenium red, μM					
	H9C2		SH-SY5Y		A7R5	
	100 μM	20 μM	100 μM	20 μM	100 μM	20 μM
Caffeine	97 ± 2	80 ± 5	Not tested	Not tested	Not tested	Not tested
3	70 ± 6	45 ± 5	Not tested	Not tested	Not tested	Not tested
5	71 ± 5	30 ± 5	62 ± 2	17 ± 6	71 ± 5	30 ± 5
7	74 ± 1	65 ± 9	82 ± 2	63 ± 10	Not tested	Not tested
11	77 ± 2	53 ± 8	95 ± 2	57 ± 16	Not tested	Not tested
13	80 ± 2	50 ± 2	Not tested	Not tested	Not tested	Not tested
14*	64 ± 2	65 ± 1	Not tested	Not tested	Not tested	Not tested

* Compound concentration 0.5 mM.

for triggering various Ca^{2+}-activated physiological processes by mediating of Ca^{2+} efflux from the SR/ER. The excitation–contraction coupling (ECC) process, which occurs in the myocytes, is the translation of the electrical impulse into the physical cell contraction and tissue-specific expression of RyR1 or RyR2 isoforms in skeletal or cardiac muscles.[26] Caffeine increases the activity of RyR channels, albeit not as selectively as ryanodine, and has proved particularly useful for the determination of the Ca^{2+} content in the intracellular storage organelles, such as the SR of intact cardiac muscle cells.[27]

In ruthenium red-pretreated cells, the inhibition of the compound-induced Ca^{2+} increase in a dose-dependent manner was observed. Thus, we concluded that pretreatment of cells with ruthenium red, a specific inhibitor of RyRs, blocked the compound-induced Ca^{2+} increase in a dose-dependent manner in all cell lines. Our findings suggest that similar to caffeine, the Ca^{2+} increase induced by the tested compounds involves the activation of RyRs.

To identify the source of the Ca^{2+} influx induced by the tested compounds, we studied the effect of known antagonist of Ca^{2+} channels, namely, the classical and structurally different L-type Ca^{2+} channel antagonist amlodipine. We measured the percentage of inhibition of Ca^{2+} response induction caused by the studied derivatives in cells pretreated with amlodipine. Our results showed an inhibitory effect only on H9C2 cardiomyocyte cells, indicating that the L-type Ca^{2+} channels are responsible for the Ca^{2+} influx. Moreover, the effect caused by compound **3** was not blocked, which indicates a different mechanism of action. In A7R5 and neuroblastoma cells, amlodipine does not have an inhibitory effect on the compound-induced increase in $[Ca^{2+}]_i$, which led us to conclude that in this case, the L-type Ca^{2+} channels are not involved in the Ca^{2+} influx (Table 6).

Because the SH-SY5Y cell line possesses both L- and N-type voltage-dependent Ca^{2+} channels, these cells were used to test the potential activation of the N-type channels by ethynylxanthines. According to our data, none of compounds **3**–**18** can compete with ω-conotoxin (a classical and structurally different N-type Ca^{2+} channel blocker). In other words, the N-type Ca^{2+} channels were not involved in the Ca^{2+} influx in neuroblastoma cells.

Table 6. Role of L-type Ca^{2+} channel

Compound*	Amlodipine, μM					
	H9C2		SH-SY5Y		A7R5	
	100 μM	20 μM	100 μM	20 μM	100 μM	20 μM
Caffeine	100 ± 4	100 ± 2	Not tested	Not tested	Not tested	Not tested
3	100 ± 5	59 ± 18	Not tested	Not tested	Not tested	Not tested
5	–**	–	–	–	–	–
7	60 ± 5	11 ± 3	–	–	Not tested	Not tested
11	75 ± 7	13 ± 8	–	–	Not tested	Not tested
13	69 ± 5	19 ± 8	Not tested	Not tested	Not tested	Not tested
14	100 ± 2	47 ± 8	Not tested	Not tested	Not tested	Not tested

* Compound concentration 0.5 mM.
** "–" – no effect.

Convenient synthetic protocols for the preparation of various 8-ethynyl-substituted caffeine and pentoxifylline derivatives were successfully elaborated. Taken together, the bioactivity data mentioned above indicates that the ethynylxanthine pharmacophore is very sensitive to any structural modifications. Caffeine, pentoxifylline, and even Temodar (a widely used drug for brain cancer treatment) exhibit no or slight cytotoxicity against all the studied cell lines. In fact, the studied malignant cells are more sensitive to Proxyfeine (IC_{50} 96–283 μM). We have discovered that 8-ethynylxanthines have a strong ability to suppress cancer cell growth in human breast adenocarcinoma, neuroblastoma, and especially glioma and lymphoma cell lines with IC_{50} values up to 4.7 μM. These novel caffeine derivatives exhibit the ability to selectively inhibit MMP-2 (gelatinase A) up to 52%. In addition, 8-[(1-aminocyclohexyl)ethynyl]-3,7-dimethyl-1*H*-purine-2,6(3*H*,7*H*)-dione inhibits MMP-10 activity up to 53%. According to the data obtained from the *in vitro* angiogenesis inhibition studies, 8-[(1-aminocyclohexyl)ethynyl]-3,7-dimethyl-1-(5-oxohexyl)-1*H*-purine-2,6(3*H*,7*H*)-dione and 1,3,7-trimethyl-8-(phenylethynyl)-1*H*-purine-2,6(3*H*,7*H*)-dione exhibit the ability to suppress angiogenesis by 38% and 100%, respectively, at a concentration of 20 μM. There is no direct correlation between angiogenesis and MMP inhibition, indicating that the tested compounds modulate the formation of new blood vessels by another mechanism. The Ca^{2+} channel activity induced by the novel ethynylxanthines strongly depends on the nature of the substituents. Consequently, both agonists and antagonists of Ca^{2+} channels were discovered. The studied compounds were more active antagonists than the reference compounds (caffeine, pentoxifylline, Temodar, and Proxyfeine), but, notably, were thousands of times less active than the well-known drug amlodipine in the smooth muscle A7R5 cell line. Latter result suggested that the studied derivatives do not have a strong influence on blood pressure.

The Ca^{2+} channel agonist activity of newly synthesized compounds results from their influence on receptor-operated Ca^{2+} channels, thereby triggering the activation of RyRs in the studied cell lines. Furthermore, activation of L-channels was observed in only cardiomyoblasts. Notably, N-channels were not activated in the nervous cells. Finally, it can be concluded that the obtained data provide an opportunity to further modify ethynylxanthenes in order to find a lead compound with strong antitumor activity for the treatment of cancer. In addition, these results support the therapeutic potential of the discovered compounds to treat diseases with dysregulated Ca^{2+}channel activity, such as essential tremor, pain, neuropathic pain, depression, sleep disorders, certain types of cancer, and sexual dysfunction.

Experimental

IR spectra were recorded on a Shimadzu Prestige-21 FTIR spectrometer in thin films. ^1H and ^{13}C NMR spectra (400 and 101 MHz, respectively) were recorded on a Bruker Avance Neo spectrometer at 298 K in $CDCl_3$ or DMSO-d_6. TMS was used as internal standard. Mass

spectra were recorded on an Acquity UPLC (ESI) instrument. HRMS (ESI) were recorded on a Waters Synapt GII Q-ToF UPLC/MS system. Elemental analyses were performed on a Carlo Erba 1108 apparatus. Melting points were measured on an Optimelt apparatus and were not corrected. Thin-layer chromatography (TLC) was performed using Merck Silica gel 60 F_{254} plates and visualized by UV (254 nm) fluorescence. ZEOCHEM silica gel (ZEOprep 60/35–70 microns – SI23501) was used for column chromatography.

All reagents and solvents were purchased from commercial suppliers and used without further purification, unless otherwise stated.

8-Bromo-1,3,7-trimethyl-3,7-dihydro-1*H*-purine-2,6-dione (1).[15] Caffeine (10.0 g, 0.05 mol) and NBS (17.6 g, 0.10 mol) were added to freshly distilled CH_2Cl_2 (150 ml) charged into a round-bottom flask. When the solids dissolved in the solvent, H_2O (50 ml) was added and the reaction mixture was stirred for 5 days. Then cold 2 M aq NaOH (30 ml) was added and the mixture was shaken till decolorization. The organic layer was separated, washed with H_2O (2×200 ml), dried over Na_2SO_4, filtered, and evaporated under reduced pressure to give the title compound as colorless solid. Yield 13.5 g (99%). ^{1}H NMR spectrum ($CDCl_3$), δ, ppm: 3.41 (3H, s, 1-NCH_3); 3.57 (3H, s, 3-NCH_3); 3.97 (3H, s, 7-NCH_3).

8-Bromo-3,7-dimethyl-1-(5-oxohexyl)-3,7-dihydro-1*H*-purine-2,6-dione (2).[15] Pentoxifylline (13.4 g, 0.05 mol) and NBS (17.6 g, 0.10 mol) were added into a round-bottom flask containing freshly distilled CH_2Cl_2 (150 ml). When the solids dissolved, H_2O (50 ml) was added and the reaction mixture was stirred for 5 days. Then cold 2 M aq NaOH (30 ml) was added and the mixture was shaken till decolorization. The organic layer was separated, washed with H_2O (2×200 ml), dried over Na_2SO_4, filtered, and evaporated under reduced pressure to give the title compound as colorless solid. Yield 16.95 g (95%). ^{1}H NMR spectrum ($CDCl_3$), δ, ppm (*J*, Hz): 1.61–1.67 (4H, m, C(O)CH_2($C\underline{H}_2$)$_2$); 2.14 (3H, s, CH_3C(O)); 2.49 (2H, t, *J* = 7.0, CH_3C(O)$C\underline{H}_2$); 3.54 (3H, s, 3-NCH_3); 3.95 (3H, s, 7-NCH_3); 3.99 (2H, t, *J* = 7.0, $(CH_2)_3C\underline{H}_2N$).

Synthesis of 8-ethynylxanthines 3–18 (General procedure). Method I. Dry *N*-methylpyrrolidine (NMP) or DMF (40 ml) was added to a mixture of $PdCl_2$ (113 mg, 0.637 mmol), CuI (242 mg, 1.27 mmol), and Ph_3P (333 mg, 1.27 mmol). The reaction mixture was stirred at 40°C for 15 min with simultaneous purge with argon. Then a solution of 8-bromo-1,3,7-trimethyl-3,7-dihydro-1*H*-purine-2,6-dione (**1**) (1.73 g, 6.37 mmol) and the appropriate alkyne (9.56 mmol) in dry DIEA (3.6 ml) was added and stirring was continued at 50°C for 24 h. After cooling to room temperature, the reaction mixture was poured into EtOAc (300 ml), washed with brine (80 ml) containing aq NH_3 (0.5 ml) and stirred at room temperature for the additional 30 min. The aqueous phase was separated, and the organic phase was washed with brine (3×80 ml), dried over anhydrous Na_2SO_4, and concentrated under reduced pressure. The crude product was purified by flash chromatography on silica gel using a mixture of H_2O (containing 0.1% HCl) – MeCN (5–70%) as eluent to give the title compound

Method II. Dry NMP or $AcNMe_2$ (40 ml) was added to a mixture of $Pd(OAc)_2$ (100 mg, 0.446 mmol), CuI (169 mg, 0.868 mmol), and Ph_3P (233 mg, 0.890 mmol). The reaction mixture was stirred for 15 min at 40°C with simultaneous purge with argon. Then a solution of 8-bromo-1,3,7-trimethyl-3,7-dihydro-1*H*-purine-2,6-dione (**1**) (1.21 g, 4.46 mmol) and the appropriate alkyne (0.65 ml, 6.69 mmol) in dry DIEA (4.0 ml) was added and stirring was continued at 55°C for 24 h. Isolation of the product as in method I.

Method III. Dry NMP (10 ml) was added to a mixture of $Pd(OAc)_2$ (100 mg, 0.446 mmol), CuI (169 mg, 0.868 mmol), and Ph_3P (233 mg, 0.890 mmol). The reaction mixture was stirred for 15 min at 40°C with simultaneous purge with argon. Then a solution of 8-bromo-1,3,7-trimethyl-3,7-dihydro-1*H*-purine-2,6-dione (**1**) or 8-bromo-3,7-dimethyl-1-(5-oxohexyl)-3,7-dihydro-1*H*-purine-2,6-dione (**2**) (4.46 mmol) and the appropriate alkyne (6.69 mmol) and dry DIEA (4.0 ml) in NMP (10 ml) and PhMe (10 ml) was added and stirring was continued at 50°C for 24 h. Isolation of the product as in method I.

Method IV. A vial was charged with $Pd(PPh_3)_4$ (346 mg, 0.3 mmol), $PdCl_2$ (51 mg, 0.3 mmol), Ph_3P (157 mg, 0.6 mmol), CuI (58 mg, 0.3 mmol), 8-bromo-1,3,7-trimethyl-3,7-dihydro-1*H*-purine-2,6-dione (**1**) or 8-bromo-3,7-dimethyl-1-(5-oxohexyl)-3,7-dihydro-1*H*-purine-2,6-dione (**2**) (15.0 mmol), the appropriate alkyne (21.0 mmol), DIEA (5.0 ml), and EtOAc (70 ml). The reaction mixture was stirred for 15 min at 40°C with simultaneous purge with argon. Then reaction mixture was stirred for additional 2–4 h. After cooling to room temperature, the reaction mixture was filtered through a silica gel pad and washed with EtOAc (200 ml). Then solvent was evaporated under reduced pressure. The crude product was purified by flash chromatography on silica gel using mixture of H_2O (containing 0.1% HCl) – MeCN (5–70%).

8-(3-Hydroxy-3-methylbut-1-yn-1-yl)-1,3,7-trimethyl-3,7-dihydro-1*H*-purine-2,6-dione (3).[28] Yield 0.73 g (42%, method I), 0.38 g (31%, method II), 0.88 g (72%, method III), 2.26 g (55%, method IV), colorless solid, mp 180–182°C. ^{1}H NMR spectrum ($CDCl_3$), δ, ppm: 1.63 (6H, s, $2CH_3$); 3.36 (3H, s, 1-NCH_3); 3.51 (3H, s, 3-NCH_3); 3.52 (1H, br. s, OH); 3.90 (3H, s, 7-NCH_3). ^{13}C NMR spectrum ($CDCl_3$), δ, ppm: 28.0; 29.8; 30.8; 32.9; 65.1; 69.6; 102.5; 107.5; 135.0; 147.4; 151.5; 154.6.

8-[(1-Hydroxycyclohexyl)ethynyl]-1,3,7-trimethyl-3,7-dihydro-1*H*-purine-2,6-dione (4).[28] Yield 0.19 g (11%, method II), 0.85 g (49%, method III), 0.94 g (54%, method IV), colorless solid, mp 194–196°C. ^{1}H NMR spectrum ($CDCl_3$), δ, ppm: 1.24–1.33 (1H, m, CH_2 cyclohexane); 1.48–1.57 (3H, m, CH_2 cyclohexane); 1.66–1.75 (4H, m, CH_2 cyclohexane); 1.94–2.02 (2H, m, CH_2 cyclohexane); 3.30 (1H, br. s, OH); 3.34 (3H, s, 1-NCH_3); 3.49 (3H, s, 3-NCH_3); 3.89 (3H, s, 7-NCH_3). ^{13}C NMR spectrum ($CDCl_3$), δ, ppm: 22.9; 24.8; 27.9; 29.7; 32.9; 39.2; 68.6; 71.5; 102.0; 107.4; 135.1; 147.3; 151.4; 154.5. Mass spectrum, *m*/*z*: 317 $[M+H]^+$. Found, *m*/*z*: 317.1621 $[M+H]^+$. $C_{16}H_{21}N_4O_3$. Calculated, *m*/*z*:

317.1535. Found: C 60.71; H 6.35; N 17.30. $C_{16}H_{20}N_4O_3$. Calculated, %: C 60.75; H 6.37; N 17.71.

8-[(1-Aminocyclohexyl)ethynyl]-1,3,7-trimethyl-3,7-dihydro-1*H*-purine-2,6-dione (5). Yield 0.12 g (7%, method I), 0.27g (16%, method II), 0.74 g (43%, method III), 0.83g (48%, method IV), colorless solid, mp 187–189°C. IR spectrum, ν, cm^{-1}: 1042, 1224, 1429, 1544, 1662, 1704, 2228, 2856, 2933. ^{1}H NMR spectrum ($CDCl_3$), δ, ppm: 1.20–1.29 (1H, m, CH_2 cyclohexane); 1.48–1.67 (5H, m, CH_2 cyclohexane); 1.72–1.77 (2H, m, CH_2 cyclohexane); 1.81 (2H, br. s, NH_2); 1.93–1.97 (2H, m, CH_2 cyclohexane); 3.39 (3H, s, 1-NCH_3); 3.55 (3H, s, 3-NCH_3); 3.98 (3H, s, 7-NCH_3). ^{13}C NMR spectrum ($CDCl_3$), δ, ppm: 23.2; 25.1; 27.9; 29.7; 33.0; 39.6; 50.4; 70.9; 104.5; 107.6; 135.8; 147.6; 151.5; 154.8. Found, *m*/*z*: 316.1779 $[M+H]^+$. $C_{16}H_{22}N_5O_2$. Calculated, *m*/*z*: 316.1768.

8-[3-(Dimethylamino)prop-1-yn-1-yl]-1,3,7-trimethyl-3,7-dihydro-1*H*-purine-2,6-dione hydrochloride (6). Yield 0.06 g (4%, method II), 0.71 g (47%, method III), 0.87 g (58%, method IV), colorless solid, mp 197–199°C (decomp.). ^{1}H NMR spectrum (DMSO-d_6), δ, ppm: 2.88 (6H, s, $N(CH_3)_2$); 3.21 (3H, s, 1-NCH_3); 3.38 (3H, s, 3-NCH_3); 3.96 (3H, s, 7-NCH_3); 4.50 (2H, s, CH_2N). ^{13}C NMR spectrum (DMSO-d_6), δ, ppm: 27.6; 29.3; 33.0; 41.6; 45.7; 76.4; 87.1; 107.6; 132.9; 146.8; 150.7; 154.0. Mass spectrum, *m*/*z*: 277 $[M+H]^+$. Found, *m*/*z*: 276.1463 $[M+H]^+$. $C_{13}H_{18}N_5O_2$. Calculated, *m*/*z*: 276.1382. Found, %: C 47.37; H 5.64; N 20.96. $C_{13}H_{17}N_5O_2 \cdot 1.5HCl$. Calculated, %: C 47.32; H 5.65; N 21.22.

8-{3-[Bis(2-methoxyethyl)amino]prop-1-yn-1-yl}-1,3,7-trimethyl-3,7-dihydro-1*H*-purine-2,6-dione (7). Yield 0.2 g (10%, method II), 0.59 g (30%, method III), 0.65 g (33%, method IV), brownish foam. ^{1}H NMR spectrum ($CDCl_3$), δ, ppm (*J*, Hz): 2.79 (4H, t, *J* = 5.5, $2NC\underline{H}_2CH_2O$); 3.31 (6H, s, $2OCH_3$); 3.34 (3H, s, 1-NCH_3); 3.48 (4H, t, *J* = 5.5, $2NCH_2C\underline{H}_2O$); 3.51 (3H, s, 3-NCH_3); 3.82 (2H, s, CH_2N); 3.96 (3H, s, 7-NCH_3). ^{13}C NMR spectrum ($CDCl_3$), δ, ppm: 27.8; 29.6; 33.0; 44.1; 53.5; 58.7; 70.9; 73.2; 94.1; 107.5; 135.4; 147.5; 151.4; 154.7. Mass spectrum, *m*/*z*: 364 $[M+H]^+$.

1,3,7-Trimethyl-8-[3-(pyrrolidin-1-yl)prop-1-yn-1-yl]-3,7-dihydro-1*H*-purine-2,6-dione (8). Yield 0.13 g (8%, method I), 0.86 g (52%, method III), 0.94 g (57%, method IV), colorless solid, mp 149–150°C. ^{1}H NMR spectrum ($CDCl_3$), δ, ppm: 1.83–1.86 (4H, m, $2C\underline{H}_2CH_2N$); 2.68–2.72 (4H, m, $2CH_2C\underline{H}_2N$); 3.39 (3H, s, 1-NCH_3); 3.56 (3H, s, 3-NCH_3); 3.75 (2H, s, CH_2N); 4.00 (3H, s, 7-NCH_3). ^{13}C NMR spectrum ($CDCl_3$), δ, ppm: 23.8; 27.9; 29.7; 33.1; 43.6; 52.7; 72.6; 94.5; 107.6; 135.4; 147.6; 151.5; 154.8. Mass spectrum, *m*/*z*: 302 $[M+H]^+$. Found, *m*/*z*: 302.1623 $[M+H]^+$. $C_{15}H_{20}N_5O_2$. Calculated, *m*/*z*: 302.1539.

1,3,7-Trimethyl-8-[3-(piperidin-1-yl)prop-1-yn-1-yl]-3,7-dihydro-1*H*-purine-2,6-dione (9). Yield 0.60 g (35%, method III), 0.52 g (30%, method IV), colorless solid, mp 137–138°C. ^{1}H NMR spectrum ($CDCl_3$), δ, ppm: 1.40–1.48 (2H, m, $CH_2C\underline{H}_2CH_2$); 1.60–1.67 (4H, m, $C\underline{H}_2CH_2C\underline{H}_2$); 2.54–2.60 (4H, m, $2NC\underline{H}_2CH_2$); 3.39 (3H, s, 1-NCH_3); 3.55 (3H, s, 3-NCH_3); 3.60 (2H, s, CH_2N); 4.00 (3H, s, 7-NCH_3). ^{13}C NMR spectrum ($CDCl_3$), δ, ppm: 23.6; 25.8; 27.9; 28.0; 29.8; 48.3; 53.4; 73.2; 94.2; 107.6; 135.5; 147.6; 151.5; 154.8. Mass spectrum, *m*/*z*: 316 $[M+H]^+$. Found, *m*/*z*: 316.1779 $[M+H]^+$. $C_{16}H_{22}N_5O_2$. Calculated, *m*/*z*: 316.1695.

8-[3-(Azepan-1-yl)prop-1-yn-1-yl]-1,3,7-trimethyl-3,7-dihydro-1*H*-purine-2,6-dione hydrate (10). Yield 0.61 g (34%, method III), brownish solid, mp 99–101°C. ^{1}H NMR spectrum ($CDCl_3$), δ, ppm (*J*, Hz): 1.61–1.64 (4H, m, $CH_2C\underline{H}_2C\underline{H}_2CH_2$); 1.70–1.76 (4H, m, $C\underline{H}_2CH_2CH_2C\underline{H}_2$); 2.81 (4H, t, *J* = 6.7, $2NCH_2$); 3.39 (3H, s, 1-NCH_3); 3.55 (3H, s, 3-NCH_3); 3.74 (2H, s, CH_2N); 4.01 (3H, s, 7-NCH_3). ^{13}C NMR spectrum ($CDCl_3$), δ, ppm: 26.6; 27.9; 28.0; 29.7; 33.1; 48.7; 55.3; 72.9; 93.2; 107.6; 135.4; 147.6; 151.5; 154.8. Mass spectrum, *m*/*z*: 330 $[M+H]^+$. Found, *m*/*z*: 330.1933 $[M+H]^+$. $C_{17}H_{24}N_5O_2$. Calculated, *m*/*z*: 330.1852. Found, %: C 60.35; H 6.95; N 20.31. $C_{17}H_{23}N_5O_2 \cdot 0.5H_2O$. Calculated, %: C 60.64; H 7.15; N 20.69.

1,3,7-Trimethyl-8-[3-(morpholin-4-yl)prop-1-yn-1-yl]-3,7-dihydro-1*H*-purine-2,6-dione (11). Yield 0.66 g (38%, method III), colorless solid, mp 88–190°C. ^{1}H NMR spectrum ($CDCl_3$), δ, ppm (*J*, Hz): 2.64 (4H, t, *J* = 4.8, $2NCH_2$); 3.40 (3H, s, 1-NCH_3); 3.56 (3H, s, 3-NCH_3); 3.64 (2H, s, CH_2N); 3.76 (4H, t, *J* = 4.8, $2CH_2O$); 4.01 (3H, s, 7-NCH_3). ^{13}C NMR spectrum ($CDCl_3$), δ, ppm: 28.0; 29.7; 33.2; 47.8; 52.3; 66.7; 73.7; 93.1; 107.7; 135.2; 147.6; 151.5; 154.8. Mass spectrum, *m*/*z*: 318 $[M+H]^+$.

8-(3-Hydroxy-3-methylbut-1-yn-1-yl)-3,7-dimethyl-1-(5-oxohexyl)-3,7-dihydro-1*H*-purine-2,6-dione (12). Yield 0.66 g (44%, method III), 0.71 g (47%, method IV), brownish solid, mp 96–98°C. IR spectrum, ν, cm^{-1}: 761, 969, 1171, 1217, 1428, 1545, 1601, 1661, 1703, 2238, 2946, 3416. ^{1}H NMR spectrum ($CDCl_3$), δ, ppm (*J*, Hz): 1.62–1.66 (4H, m, $CH_2(C\underline{H}_2)_2CH_2N$); 1.65 (6H, s, $2CH_3$); 2.12 (3H, s, CH_3CO); 2.48 (2H, t, *J* = 7.1, $CH_3C(O)C\underline{H}_2$); 2.72 (1H, br. s, OH); 3.53 (3H, s, 3-NCH_3); 3.96 (3H, s, 7-NCH_3); 3.97 (2H, t, *J* = 7.1, $(CH_2)_3C\underline{H}_2N$). ^{13}C NMR spectrum ($CDCl_3$), δ, ppm: 20.9; 27.3; 29.7; 29.9; 30.9; 33.0; 40.9; 43.1; 65.4; 70.0; 102.2; 107.7; 135.1; 147.6; 151.2; 154.6; 208.7. Mass spectrum, *m*/*z*: 361 $[M+H]^+$. Found, *m*/*z*: 361.1884 $[M+H]^+$. $C_{18}H_{25}N_4O_4$. Calculated, *m*/*z*: 361.1798.

8-[(1-Hydroxycyclohexyl)ethynyl]-3,7-dimethyl-1-(5-oxohexyl)-3,7-dihydro-1*H*-purine-2,6-dione (13). Yield 0.70 g (42%, method III), colorless solid, mp 126–128°C. IR spectrum, ν, cm^{-1}: 761, 969, 1076, 1170, 1222, 1339, 1428, 1486, 1546, 1601, 1661, 1708, 2231, 2858, 2936, 3431. ^{1}H NMR spectrum ($CDCl_3$), δ, ppm (*J*, Hz): 1.27–1.37 (1H, m, CH_2 cyclohexane); 1.54–1.80 (11H, m, CH_2 cyclohexane, $CH_2(C\underline{H}_2)_2CH_2N$); 2.02–2.08 (2H, m, CH_2 cyclohexane); 2.13 (3H, s, CH_3CO); 2.48 (2H, t, *J* = 7.1, $CH_3C(O)C\underline{H}_2$); 3.54 (3H, s, 3-NCH_3); 3.97 (3H, s, 7-NCH_3); 3.99 (2H, t, *J* = 7.1, $(CH_2)_3C\underline{H}_2N$). ^{13}C NMR spectrum ($CDCl_3$), δ, ppm: 20.9; 23.0; 24.9; 27.4; 29.7; 29.9; 33.1; 39.3; 40.9; 43.1; 69.0; 72.0; 101.5; 107.8; 135.3; 147.6; 151.2; 154.6; 208.6. Mass spectrum, *m*/*z*: 401 $[M+H]^+$. Found, *m*/*z*: 401.2196 $[M+H]^+$. $C_{21}H_{29}N_4O_4$. Calculated, *m*/*z*: 401.2111.

8-[(1-Aminocyclohexyl)ethynyl]-3,7-dimethyl-1-(5-oxohexyl)-3,7-dihydro-1*H*-purine-2,6-dione (14). Yield 0.75 g (45%, method III), colorless solid, mp > 200°C. ^{1}H NMR spectrum ($CDCl_3$), δ, ppm: 1.24–1.34 (1H, m, CH_2 cyclohexane);

1.61–1.72 (7H, m, CH_2 cyclohexane); 1.81–1.84 (2H, m, $CH_2(C\underline{H}_2)_2CH_2N$); 1.95–2.01 (2H, m, $CH_2(C\underline{H}_2)_2CH_2N$); 2.13 (3H, s, CH_3CO); 2.34–2.38 (2H, m, CH_2 cyclohexane); 2.48 (2H, t, J = 6.8, $CH_3C(O)C\underline{H}_2$); 3.49 (3H, s, 3-NCH_3); 3.95 (2H, t, J = 6.8, $(CH_2)_3C\underline{H}_2N$); 4.01 (3H, s, 7-$NCH_3$); 9.29 (2H, br. s, NH_2). ^{13}C NMR spectrum ($CDCl_3$), δ, ppm: 20.9; 22.5; 24.1; 27.3; 25.1; 29.7; 29.9; 33.5; 35.9; 41.0; 43.1; 53.6; 75.7; 93.9; 108.0; 133.8; 147.4; 150.9; 154.4; 208.6. Mass spectrum, *m*/*z*: 400 $[M+H]^+$. Found, *m*/*z*: 401.2198 $[M+2]^+$. $C_{21}H_{31}N_5O_3$. Calculated, *m*/*z*: 401.2270.

8-{3-[Bis(2-methoxyethyl)amino]prop-1-yn-1-yl}-3,7-dimethyl-1-(5-oxohexyl)-3,7-dihydro-1*H*-purine-2,6-dione (15). Yield 0.65 g (35%, method III), brownish foam. IR spectrum, ν, cm^{-1}: 1118, 1438, 1547, 1661, 1702, 2950, 3415. ^{1}H NMR spectrum ($CDCl_3$), δ, ppm (*J*, Hz): 1.60–1.65 (4H, m, $CH_2(C\underline{H}_2)_2CH_2N$); 2.11 (3H, s, CH_3CO); 2.47 (2H, t, J = 6.9, $CH_3C(O)C\underline{H}_2$); 3.38 (9H, s, 3-NCH_3, 2OCH_3); 3.43–3.56 (4H, m, 2$NC\underline{H}_2CH_2O$); 3.56 (3H, s, 7-NCH_3); 3.92–3.97 (4H, m, 2$NCH_2C\underline{H}_2O$); 3.97 (2H, t, J = 6.9, $(CH_2)_3C\underline{H}_2N$); 4.11 (2H, s, CH_2N). ^{13}C NMR spectrum ($CDCl_3$), δ, ppm: 20.9; 27.4; 29.8; 31.9; 40.7; 43.1; 54.2; 58.8; 63.0; 66.5; 71.0; 76.9; 107.2; 110.3; 143.1; 147.3; 148.1; 151.3; 155.1; 208.6. Mass spectrum, *m*/*z*: 448 $[M+H]^+$. Found, *m*/*z*: 448.2552 $[M+H]^+$. $C_{22}H_{34}N_5O_5$. Calculated, *m*/*z*: 448.2482.

3,7-Dimethyl-1-(5-oxohexyl)-8-[3-(pyrrolidin-1-yl)prop-1-yn-1-yl]-3,7-dihydro-1*H*-purine-2,6-dione (16). Yield 0.66 g (41%, method III), brownish foam. IR spectrum, ν, cm^{-1}: 769, 1223, 1436, 1539, 1653, 1700, 2803, 2961. ^{1}H NMR spectrum ($CDCl_3$), δ, ppm (*J*, Hz): 1.61–1.70 (4H, m, $CH_2(C\underline{H}_2)_2CH_2N$); 1.82–1.86 (4H, m, CH_2 pyrrolidine); 2.13 (3H, s, CH_3CO); 2.49 (2H, t, J = 7.0, $CH_3C(O)C\underline{H}_2$); 2.64–2.68 (4H, m, CH_2 pyrrolidine); 3.48 (2H, s, CH_2N); 3.58 (3H, s, 3-NCH_3); 3.93 (3H, s, 7-NCH_3); 4.01 (2H, t, J = 7.0, $(CH_2)_3C\underline{H}_2N$). ^{13}C NMR spectrum ($CDCl_3$), δ, ppm: 20.8; 23.9; 27.3; 29.6; 29.9; 33.6; 40.9; 43.0; 43.3; 52.7; 77.6; 85.1; 108.4; 133.0; 147.4; 151.0; 154.5; 208.5. Mass spectrum, *m*/*z*: 386 $[M+H]^+$. Found, *m*/*z*: 386.2194 $[M+H]^+$. $C_{20}H_{28}N_5O_3$. Calculated, *m*/*z*: 386.2114.

3,7-Dimethyl-1-(5-oxohexyl)-8-[3-(piperidin-1-yl)prop-1-yn-1-yl]-3,7-dihydro-1*H*-purine-2,6-dione (17). Yield 0.65 g (39%, method III), colorless solid, mp 182–184°C. ^{1}H NMR spectrum ($CDCl_3$), δ, ppm (*J*, Hz): 1.34–1.48 (1H, m, CH_2 piperidine); 1.58–1.66 (4H, m, $CH_2(C\underline{H}_2)_2CH_2N$); 1.90–1.93 (3H, m, CH_2 piperidine); 2.11 (3H, s, CH_3CO); 2.21–2.29 (2H, m, CH_2 piperidine); 2.47 (2H, t, J = 7.0, $CH_3C(O)C\underline{H}_2$); 2.94–2.97 (2H, m, CH_2 piperidine); 3.51 (3H, s, 3-NCH_3); 3.60–3.63 (2H, m, CH_2 piperidine); 3.97 (2H, t, J = 7.0, $(CH_2)_3C\underline{H}_2N$); 4.07 (3H, s, 7-$NCH_3$); 4.22 (2H, s, CH_2N). ^{13}C NMR spectrum ($CDCl_3$), δ, ppm: 20.8; 21.5; 22.7; 27.3; 29.6; 29.9; 33.7; 40.9; 43.0; 46.7; 52.6; 78.7; 84.6; 108.5; 133.1; 147.5; 151.0; 154.5; 208.5. Mass spectrum, *m*/*z*: 400 $[M+H]^+$. Found, *m*/*z*: 400.2357 $[M+H]^+$. $C_{21}H_{29}N_5O_3$. Calculated, *m*/*z*: 400.2270.

1,3,7-Trimethyl-8-(phenylethynyl)-3,7-dihydro-1*H*-purine-2,6-dione (18).[29] Yield 0.58 g (36%, method III), colorless solid. ^{1}H NMR spectrum ($CDCl_3$), δ, ppm: 3.43 (3H, s, 1-NCH_3); 3.61 (3H, s, 3-NCH_3); 4.10 (3H, s, 7-NCH_3); 7.39–7.46 (3H, m, H Ph); 7.61–7.63 (2H, m, H Ph).

***In vitro* cytotoxicity assay**. Monolayer tumor cell lines: MDA-MB-435s (human melanoma), H9C2 (rat embrio cardiomyoblasts), MCF-7 (human breast adenocarcinoma, estrogen-positive), HepG2 (human hepatocellular carcinoma), SH-SY5Y (human neuroblastoma), C6 (rat glioma), U937 (human histiocytic leukemia), and A549 (human lung carcinoma). The cells were seeded in 96-well plates in DMEM and cultivated for 72 h while exposed to different concentrations of the compounds. Cell viability was measured *via* MTT assay.[30] Briefly, after incubation with the compounds, the culture medium was removed, and fresh medium containing 0.2 mg/ml MTT was added. After incubation (3 h, 37°C, 5% CO_2), the MTT-containing medium was removed, and 200 μl of DMSO was immediately added to each sample. The samples were assessed at 540 nm on a Tecan Infinite1000 microplate reader. The half-maximal inhibitory concentration (IC_{50}) of each compound was calculated using GraphPad Prism 3.0.

MMP assay. Inhibitors of matrix metalloproteinase enzymes were detected with the use of MMP Inhibitor Fluorimetric Profiling kit (Biomol, USA) accordingly to manufacturer's instructions. MMP activity assays were performed in 96-well plates using the recombinant human MMP-1–10, MMP-12–14 catalytic domains and OmniMMP™ fluorogenic substrate Mca-Pro-Leu-Gly-Leu-Dpa-Ala-Arg-NH_2. The test compounds (20 μM) were dissolved in DMSO. NNGH (*N*-isobutyl-*N*-(4-methoxyphenylsulfonyl)glycyl hydroxamic acid) was used as a prototypic control inhibitor. The rate of substrate hydrolysis was determined by fluorescence intensity measuring for 10 min at 37°C temperature using a fluorescence plate reader (Tecan infinite M1000, Austria) with excitation at 328 nm and emission at 420 nm. Data analysis was performed using program GraphPad Prism 3.0.

***In vitro* angiogenesis assay**. An *in vitro* Matrigel assay was performed according to the literature methodology.[31] HUVEC cells were grown in Vascular Cell Basal medium with 2% fetal bovine serum, bovine brain extract, hydrocortisone, human endothelial growth factor, and gentamicin/amphotericin B (ATCC) in incubator with 5% CO_2 and at 37°C. Matrigel was dispensed into 96-well plates (50 μl/well). Plates were incubated at 37°C for 1 h to allow polymerization of matrigel. HUVEC cultures were added into each matrigel-coated well at a final concentration of 10 000 cells/well. After 8 h incubation at 37°C cells were labeled with calcein-AM (Molecular Probes) and photographed at 4-fold magnification using an inverted fluorescence microscope (Nicon) calculating the length of capillary tubes.

Intracellular Ca^{2+} measurements. Changes in intracellular $[Ca^{2+}]_i$ concentration were studied using Fluo-4 NW Calcium Assay kit (Invitrogen, Sweden) accordingly to manufacturer's protocol. The cells A7R5, H9C2 or SH-SY5Y were seeded into 96-well plate at 10 000 cells per well and incubated for 72 h. Intracellular free Ca^{2+} concentration $[Ca^{2+}]_i$ was measured in confluent monolayers of cells with the Ca^{2+}-sensitive fluorescent

indicator Fluo 4 NW. The model for investigation of Ca^{2+} channel blocking activity caused by 8-ethynylxanthine derivatives was based on the analysis of the effect of caffeine on intracellular Ca^{2+} mobilization in H9C2 cells; accordingly, carbachol was used in case of SH-SY5Y cells and KCl effect on intracellular Ca^{2+} mobilization in A7R5 cells. The cells were preincubated with tested compounds at concentrations from 0.01 to 2 mM in the dark for 15 min. Application of caffeine (1.2 mM) for H9C2, carbachol (30 μM) for SH-SY5Y and KCl (50 mM) for A7R5 to Fluo-4NW loaded cells stimulated intracellular Ca^{2+} mobilization. In case of Ca^{2+} channel agonist activity studies Fura-4NW loaded cells were stimulated by the addition of tested compounds. Changes in $[Ca^{2+}]_i$ were measured with the fluorescence emitted at 516 nm due to alternate excitation at 494 nm using a fluorescence spectrophotometer (TECAN, Infinite M1000). Intracellular Ca^{2+} concentration ($[Ca^{2+}]_i$) was calculated from a standard curve with known amounts of free Ca^{2+} using the standard Ca^{2+}-EGTA buffering system (Calcium Calibration Buffer kit, cat. No. C-3008, Life Technologies). IC_{50} values for the tested compounds were calculated using the GraphPad Prism 3.0 software. All data are representative as the mean of four independent experiments.

Detection the role of InsP3R in the Ca^{2+} response was investigated by the InsP3Rs inhibitor 2-APB. The role of ryanodine receptor in Ca^{2+} response was investigated by ruthenium red as a potent RyR inhibitor. For detection of the role of L-type calcium channel in Ca^{2+} response, amlodipine was used as L-type Ca^{2+} channel blocker; besides, ω-conotoxin was used as N-type Ca^{2+} channel blocker. Cells were pretreated for 15 min with the corresponding inhibitor and then stimulated intracellular Ca^{2+} mobilization with tested compound.

References

1. Jemal, A.; Bray, F.; Center, M. M.; Ferlay, J.; Ward, E.; Forman, D. *Ca–Cancer J. Clin.* **2011**, *61*, 69.
2. Jemal, A.; Siegel, R.; Xu, J.; Ward, E. *Ca–Cancer J. Clin.* **2010**, *60*, 277.
3. Siegel, R. L.; Miller, K. D.; Jemal, A. *Ca–Cancer J. Clin.* **2017**, *67*, 7.
4. Siegal, T. *J. Neuro-Oncology* **2013**, *15*, 656.
5. Lampson, L. A. *Drug Discovery Today* **2009**, *14*, 185.
6. Huse, J. T.; Holland, E. C. *Nat. Rev. Cancer* **2010**, *10*, 319.
7. Wilson, K. M.; Kasperzyk, J. L.; Rider, J. R.; Kenfield, S.; van Dam, R. M.; Stampfer, M. J.; Giovannucci, E.; Mucci, L. A. *J. Nat. Cancer Inst*. **2010**, *103*, 876.
8. Geybels, M. S.; Neuhouser, M. L.; Wright, J. L.; Stott-Miller, M.; Stanford, J. L. *Cancer*, *Causes Control* **2013**, *24*, 1947.
9. Bravi, F.; Bosetti, C.; Tavani, A.; Bagnardi, V.; Gallus, S.; Negri, E.; Franceschi, S.; La Vecchia, C. *Hepatology* **2007**, *46*, 430.
10. Yamamoto, N.; Tsuchiya, H. *J. Caffeine Res*. **2011**, *1*, 163.
11. Hayashi, M.; Tsuchiya, H.; Yamamoto, N.; Karita, M.; Shirai, T.; Nishida, H.; Takeuchi, A.; Tomita, K. *Anticancer Res*. **2005**, *25*, 2399.
12. Ding, R.; Shi, J.; Pabon, K.; Scotto, K. W. *Mol. Pharmacol*. **2012**, *81*, 328.
13. Vartanyan, L. P.; Kolesova, M. B.; Gornaeva, G. F.; Pustovalov, Yu. I. *Psychopharmacol. Biol. Narcol*. [In Russian] **2005**, *5*, 1093.
14. Rybár, A.; Pfleiderer, W. *Collect. Czeh. Chem. Commun.* **1987**, *52*, 2730.
15. Soltani Rad, M. N.; Behrouz, S.; Nekoei, A.-R. *Synlett* **2012**, 1191.
16. Arsenyan, P.; Rubina, K.; Vasiljeva, J.; Belyakov, S. *Tetrahedron Lett*. **2013**, *54*, 6524.
17. Schafer, B.; Gschwind, A.; Ullrich, A. *Oncogene* **2004**, *23*, 991.
18. Yamazaki, D.; Kurisu, S.; Takenawa, T. *Cancer Sci*. **2005**, *96*, 379.
19. Ridley, A. J.; Schwartz, M. A.; Burridge, K.; Firtel, R. A.; Ginsberg, M. H.; Borisy, G.; Parsons, J. T.; Horwitz, A. R. *Science* **2003**, *302*, 1704.
20. Berridge, M. J.; Bootman, M. D.; Lipp, P. *Nature* **1998**, *395*, 645.
21. Rousseau, E.; Ladine, J.; Liu, Q.-Y.; Meissner, G. *Arch. Biochem. Biophys.* **1988**, *267*, 75.
22. Garavito-Aguilar, Z. V.; Recio-Pinto, E.; Corrales, A. V.; Zhang, J.; Blanck, T. J. J.; Xu, F. *Brain Res*. **2004**, *1011*, 177.
23. Rucins, M.; Gosteva, M.; Domracheva, I.; Kanepe-Lapsa, I.; Belyakov, S.; Plotniece, M.; Pajuste, K.; Cekavicus, B.; Jekabsone, M.; Sobolev, A.; Shestakova, I.; Plotniece, A. *Chem. Heterocycl. Compd*. **2015**, *50*, 1432. [*Khim. Geterotsikl. Soedin.* **2014**, 1557.]
24. Berridge, M. J. *Neuron* **1998**, *21*, 13.
25. Verkhratsky, A. *Physiol. Rev*. **2005**, *85*, 201.
26. Fleischer, S.; Inui, M. *Prog. Clin. Biol. Res*. **1988**, *273*, 435.
27. Thomas, N. L.; Williams, A. J. *Wiley Interdiscip. Rev.*: *Membr. Transp. Signaling* **2012**, *1*, 383.
28. Arsenyan, P.; Vasiljeva, J.; Ivanova, A.; Belyakov, S. *Mendeleev Commun*. **2019**, *29*, 96.
29. Schwarz Pharma AG. EP Patent EP1939197 A1, 2008.
30. Mosmann, T. *J. Immunol. Methods* **1983**, *65*, 55.
31. Ponce, M. L. In *Angiogenesis Protocols*; Murray, J. C., Ed.; Humana Press, 2001, p. 205.